

Activity and deactivation of Fe-MFI catalysts for benzene hydroxylation to phenol by N₂O

D. Meloni,^a R. Monaci,^a V. Solinas,^a G. Berlier,^b S. Bordiga,^b I. Rossetti,^c
C. Oliva,^c and L. Forni^{c,*}

^a Dipartimento di Scienze Chimiche, Università di Cagliari, Complesso Universitario di Monserrato, S.S. 554 Bivio per Sestu, I-09042 Cagliari, Italy

^b Dipartimento di Chimica Inorganica, Fisica e dei Materiali, Università di Torino, via P. Giuria, 7, I-10125 Torino, Italy

^c Dipartimento di Chimica Fisica ed Elettrochimica, Università di Milano, via Golgi, 19, I-20133 Milano, Italy

Received 9 July 2002; revised 4 November 2002; accepted 10 December 2002

Abstract

Isomorphously substituted Fe-MFI zeolite catalysts with various Si/Al and/or Si/Fe ratios were synthesized and characterized by many different techniques, such as ICP, XRD, SEM, TPR, microcalorimetry, FTIR, and EPR. Under standard reaction conditions the best catalyst gave 20% benzene conversion and over 90% selectivity to phenol. For Fe-ZSM5 catalysts, addition of steam to the feed improved catalyst activity, selectivity, and durability. Phenol formed onto Fe-based sites only. Active sites could very likely be composed of oxygen-bridged, extraframework binuclear Fe redox species, charge-compensating the framework Fe³⁺ or Al³⁺ ions. Surface acidity was not responsible for activity in the main reaction, but it was heavily involved in catalyst deactivation by coking. Catalyst deactivation derived mainly from the decomposition-condensation of phenol onto acid sites; the stronger the latter, the quicker was the coking rate.

© 2003 Elsevier Science (USA). All rights reserved.

Keywords: Fe-MFI catalyst; Benzene hydroxylation by N₂O; Catalyst acidity; Catalyst coking

1. Introduction

Various materials (mixed metal oxides, zeolites) have been tested as catalysts for the one step oxidation of benzene to phenol with N₂O and the most promising were MFI-structured zeolites, like Fe-silicalite or Fe-ZSM5 [1–3] (selectivity higher than 90%, up to almost 100%). A demonstrative unit was also set up by Solutia [1]. The origin of the activity of these catalysts is still controversial. According to Panov and co-workers [3–5], small extraframework Fe clusters, called α -sites, can dissociate N₂O at low temperatures. This would produce (O) _{α} species responsible for the selective oxidation of benzene to phenol. Other researchers [6] proposed that Brønsted acid sites or extraframework aluminum-based Lewis acid sites are involved, so attributing the catalytic activity to surface acidity only.

During the past years we prepared and characterized some Fe-MFI catalysts [7,8], looking for correlations be-

tween catalytic activity and α -site formation [7]. The distinction between framework and extraframework Fe sites in the catalytic material was obtained by FTIR, EXAFS, XANES, and EPR analysis, as reported in detail elsewhere [8]. Both Fe²⁺ and Fe³⁺ extraframework species were observed, with different relative concentrations, depending on the thermal treatments and on the presence of redox agents. These Fe species can be either isolated ions or dinuclear or trinuclear clusters. Polynuclear clusters were also observed [8,9].

In the present work we prepared and characterized a couple of Fe-silicalites and a couple of Fe-ZSM5 samples, both with different Fe contents, accompanied by three comparative catalysts, synthesized either in the virtual absence of Fe or in the presence of a very low amount of Fe. Activity standard tests for the direct hydroxylation of benzene by N₂O were carried out at 623 K and atmospheric pressure. The influence of iron content and of catalyst pretreatments on catalytic behavior and deactivation rate, as well as the influence of surface acidity, was investigated. Some results about the nature of coke, formed during deactivation, are also presented.

* Corresponding author.

E-mail address: lucio.forni@unimi.it (L. Forni).

2. Experimental

2.1. Catalyst preparation

Four samples of Fe-ZSM5 catalysts, referred to as Fe-Z(*x*) and three samples of Fe-silicalite catalysts, named Fe-S(*x*), were studied, the value in brackets indicating the Fe content as Fe₂O₃ wt%. All the catalysts were prepared by the hydrothermal method [7]. A low molecular weight silica source (tetraethylorthosilicate, TEOS, Aldrich, purity ≥ 98 wt%) was slowly dropped under vigorous stirring and under N₂ atmosphere into an iron-containing solution. The latter was obtained by dissolving FeCl₃ (Aldrich, purity 99.997 wt%) in anhydrous ethanol (Carlo Erba, absolute grade, further dehydrated over predried 5 Å molecular sieves). Tetrapropylammonium hydroxide (TPAOH) was added as templating agent after gel formation. TPAOH was prepared in very pure form by electro dialysis through an anionic membrane of a 1 M cathodic solution of the bromide (TPABr, Aldrich, purity ≥ 98 wt%) and using a 25 wt% aqueous ammonia as anodic solution. For the preparation of Fe-Z(*x*) samples, triisopropylaluminum (TIPA, Fluka, purity > 98 wt%) was added together with TPAOH. Finally ethanol was removed from the mother gel by evaporation at 350 K and replaced by distilled water.

The gel solution was then loaded into PTFE-lined tumbling autoclaves, heated at 377 K for 85 h. The crystallized zeolite was carefully washed till neutrality of the filtrate, heated in air flow while temperature was increased by 0.5 °C/min up to 393 K, kept for 3 h, and then calcined in air at 823 K for 16 h, to completely eliminate the structure-directing agent.

In order to obtain the decationated form, several ion-exchange treatments were carried out at 343 K for 3 h, with a 0.1 M solution of NH₄NO₃ (Fluka, pro-analisi grade), followed by drying and calcination at 823 K. Finally, a part of the powder was treated at 873 K for 5 h in a stream of air +30–50% steam.

2.2. Catalyst characterization

Chemical composition was determined by elemental analysis, by means of a Varian Liberty 200 ICP spectrometer. X-ray powder diffraction (XRD) patterns were collected on a Philips PW 1820 powder diffractometer, using the Ni-filtered Cu-K_α radiation ($\lambda = 1.5406 \text{ \AA}$). Scanning electron microscopy (SEM) analysis was carried out by means of a Cambridge Stereoscan 150 instrument. After activation of the sample (100 mg) under air (15 cm³ min⁻¹) at 823 K (10 K min⁻¹) for 5 h and cooling to room temperature, the temperature-programmed reduction (TPR) runs were performed between 303 and 1173 K (20 K min⁻¹) in a stream of 5% H₂ in N₂ (30 cm³ min⁻¹). The H₂ consumption was evaluated by monitoring the flowing carrier gas through a hot-wire detector (HWD). BET surface area and pore size distribution were determined from N₂ adsorption isotherms at 77 K (Thermofinnigan Sorptomatic 1990 apparatus, sample out gassing at 523 K for 18 h). EPR analysis was carried out on a Bruker ELEXSYS E 500 instrument, equipped with a cryogenic unit. Spectra simulation was performed by the Bruker SimFonia program. Some relevant physicochemical properties of the catalysts are collected in Table 1.

Surface acidity was analyzed by microcalorimetry, using NH₃ as probe molecule. A Tian–Calvet heat flow calorimeter (Sétaram) equipped with a volumetric vacuum line was used for collecting the calorimetric data [10]. Each sample (100 mg) was pretreated overnight at 673 K in vacuo (10⁻³ Pa). Adsorption of ammonia was carried out at 353 K, by admitting successive doses of probe molecule and recording the thermal effect. The run was stopped at a final pressure of 133.3 Pa. After out gassing (10⁻³ Pa) for 1 h at 353 K, a second adsorption was carried out. From the difference between the two parallel adsorption isotherms, the concentration of chemisorbed species was evaluated. Distinction of the Brønsted and Lewis nature of the acid sites was obtained by FTIR analysis of preadsorbed pyridine, carried out on the samples pressed into wafers (5–8 mg/cm²) and preliminarily out gassed in vacuo at 973 K to remove adsorbed H₂O. After contacting with pyridine vapour at room temperature and out gassing at 473 K, to remove the physisorbed

Table 1
Some relevant properties of the catalysts prepared

Sample	Al ₂ O ₃ ^a (wt%)	Fe ₂ O ₃ ^a (wt%)	BET SA (m ² /g)	V _{tot} (cm ³ /g)	V _{micro} (cm ³ /g)	V _{meso} (cm ³ /g)
Fe-Z(0.07)	3.13	0.07	545	0.54	0.19	0.35
Fe-Z(0.24)	3.13	0.24	524	0.57	0.19	0.38
Fe-Z(0.00) ^c	3.11	< 0.005 ^b	501	0.53	0.18	0.36
Fe-Z(0.01) ^c	3.12	0.01	498	0.54	0.19	0.37
Fe-S(0.30)	0.06	0.30	520	0.53	0.18	0.35
Fe-S(1.91)	0.04	1.91	533	0.56	0.19	0.37
Fe-S(0.00) ^c	0.03	< 0.005 ^b	515	0.51	0.18	0.33

Specific surface area (SA) and total pore volume (V_{tot}) determined by the BET equation; micropore volume (V_{micro}) by the Horvath–Kawazoe equation and mesopore volume calculated by difference (V_{meso} = V_{tot} - V_{micro}).

^a From ICP elemental analysis.

^b Lower detection limit of ICP analysis.

^c Comparative sample.

base, the concentration of Brønsted and Lewis sites able to retain pyridine at different temperatures (823, 923, and 1073 K) was determined from the area of the corresponding bands at 1545 and 1450 cm^{-1} , respectively, by employing the extinction coefficients $\epsilon_B = 0.73 \pm 0.04 \text{ cm}/\mu\text{mol}$; $\epsilon_L = 0.64 \pm 0.04 \text{ cm}/\mu\text{mol}$, respectively, reported in [11].

2.3. Catalytic activity and coke analysis

The catalytic runs were carried out at atmospheric pressure in a continuous fixed-bed quartz microreactor at 673 K. The catalyst was pressed in wafers, ground and sieved to 60 to 100-mesh particles, and then loaded after dilution 1:2 (v/v) with quartz powder of the same particle size. Prior to each run, the catalyst was activated under air flow at 773 K for 5 h, followed by cooling to the reaction temperature in flowing helium. A preheated feed of helium, containing the reactants at benzene/ N_2O /He = 1/4/15 molar feeding ratios was then continuously passed through the catalyst bed, with time factor τ (vol of cat./overall vol flow rate of reacting gas) = 0.5 s. Samples of the effluent for analysis were collected in glass traps and cooled to 233 K by means of a cryogenic system (Lauda RK8 CS), and liquid products were analyzed by a FID HP-6890 gas chromatograph, equipped with a fused-silica capillary column (Supelco Petrocol DH 0.25 mm o.d. and 50 m long). GC-MS identification of the various products was performed on a HP-5989A apparatus.

The coke content and composition were determined after dissolution of the coked catalyst in 40% HF at room temperature, extraction of the soluble part of the carbonaceous compounds in methylene chloride, and analysis by GC-MS. The procedure is reported in detail elsewhere [10,12].

3. Results and discussion

3.1. Catalyst preparation

The insertion of Fe into the zeolitic framework is the keypoint of the preparation procedure. The first critical point is to avoid the precipitation of insoluble species during gel formation. This was achieved by slowly dropping the silica source (TEOS) into the anhydrous ethanolic solution of FeCl_3 , to form the gel before addition of the structure-directing agent (TPAOH).

A further problem arises from alkaline metal impurities, usually present in the commercial TPAOH solution, which inhibit the Fe insertion into the MFI framework. This was achieved by preparing the TPAOH by electro dialysis from the bromide, which was virtually free from alkaline ions.

3.2. Catalyst characterization

The Fe content in the final catalyst (Table 1) showed a good correspondence between nominal and analytical values, thus confirming the efficiency of the preparation

procedure in inserting the desired amount of Fe (and Al, when required) into the zeolite framework.

XRD analysis showed a pure MFI structure for every sample, with some line broadening due to the small crystal size. The latter was determined through SEM analysis, which showed nanometric ($\leq 100 \text{ nm}$) particles, composed of zeolite crystals ca. 20 nm in size. XRD analysis confirmed also the insertion of Fe into the MFI framework. Indeed, the insertion of Fe^{3+} (ionic radius 0.064 nm) into the lattice (Al^{3+} 0.050 nm and Si^{4+} 0.041 nm ionic radii) causes the expansion of the unit cell, shown as a shift in the XRD reflections [13,14]. The same linear correlation between peak shift and Fe content, reported by Ratnasamy and Kuman [15], confirmed the presence of framework Fe.

All the TPR runs were carried out under identical experimental conditions, so that the relative amount of H_2 uptaken could be deduced by the direct comparison of peak area. The typical TPR profile of Fe-S(x) samples, here shown for the Fe-S(1.91) catalyst only (Fig. 1, dotted line), presents two maxima, centered at about 643 and 823 K. The peaks are sufficiently separated to allow the identification of at least two distinct families of Fe^{3+} species. The first reduction peak lies within the same temperature interval previously found [16] for other Fe-silicalite samples and so it is easily ascribed to extraframework Fe^{3+} species. The second peak, observed at higher temperature (823 K), cannot be ascribed to framework Fe^{3+} species, because the reduction of the latter occurs at a temperature higher than 950 K. It should correspond to the reduction of charge-compensating extraframework Fe^{3+} [17]. Indeed, it has been proposed [18] that the reduction of Fe_2O_3 -type entities ($\text{Fe}^{3+} \rightarrow \text{Fe}^{2+}$) occurs between 673 and 723 K, that of charge-compensating Fe^{3+} occurs at about 873 K (which probably corresponds to the peak at 823 K in the TPR profile of Fig. 1) and that of framework iron takes place at higher temperatures. On the other hand, the two Fe-Z(x) samples gave practically a single peak only, around 823 K, showing that most of the iron is in extraframework position as charge-compensating Fe^{3+} entities.

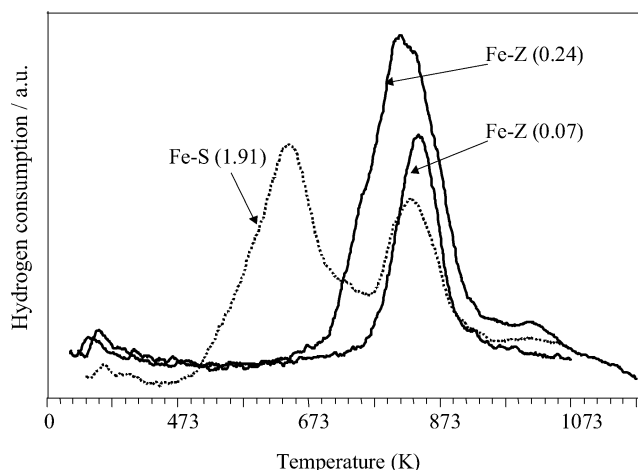


Fig. 1. TPR profiles for Fe-S(x) and Fe-Z(x) catalysts.

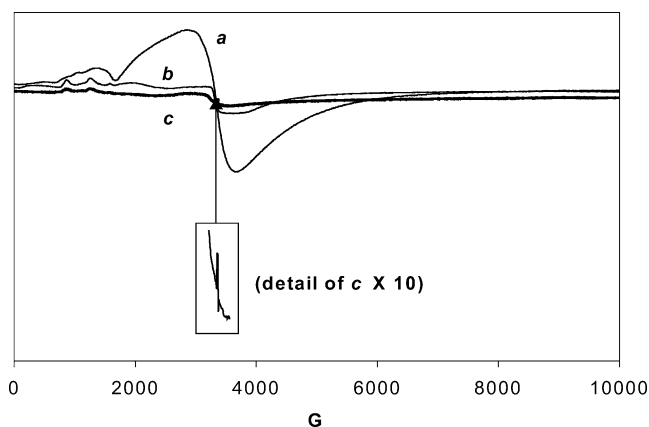


Fig. 2. EPR spectra of Fe-S(1.91) sample after steaming: (a) as prepared, (b) after reduction up to 673 K, (c) after reduction up to 873 K.

These attributions are in line with our EPR data (Figs. 2 and 3). These have been collected before and after reducing the sample in a 40 cm³/min stream of 10% H₂ in He, while increasing temperature by 10 K/min up to either 673 or 873 K, and then maintaining for 5 min, before cooling down to room temperature in pure flowing He.

The spectrum of the original, unreduced, sample included two main features, at $g > 4$ and at $g \cong 2$, respectively (Fig. 2a). After reduction of the catalyst up to 673 K, the intensity of the whole pattern decreased by ca. 80% and a better resolution was obtained in the low-field region, which resulted in two main lines, at $g = 8.2$ and 5.56 , respectively (Fig. 2b). Lines in this region have been attributed [19,20] to various mononuclear Fe³⁺ ions in more or less rhombically distorted tetrahedral sites. The spectral intensity further decreased (by ca. 92%, with respect to the unreduced sample) after reduction up to 873 K (Fig. 2c). After both reductions a change in the spectral profile took also place, indicating the simultaneous presence of different paramagnetic species, whose concentration decreases differently during the reduction. To put in evidence this behavior, we compared the shape of the spectral profile before and after TPR, by renormalizing the spectra of Fig. 2a and Fig. 2b, as shown in Fig. 3a and Fig. 3b, and subtracting the former from the latter. The spectrum of Fig. 3c was so obtained, which resulted a 110 G broad Lorentzian line, centred at $g \cong 2$ (Fig. 3d) due to the species which had undergone a less deep reduction. This line could be attributed to superparamagnetic (single-domain) particles, as those reported in our previous papers [8,9] on similar systems. They were attributed to catalytically inactive, extracrystalline, relatively large Fe oxide clusters, forming after steaming of the catalyst. After reduction up to 873 K this Lorentzian-shaped line disappeared, indicating that these species were not present anymore, probably due to full reduction to Fe²⁺ of the Fe³⁺ ions present in them.

Furthermore, after reduction up to 873 K a narrow (18 G wide) line became evident (see detail inserted in Fig. 2). The intensity of the latter decreased with increasing temperature,

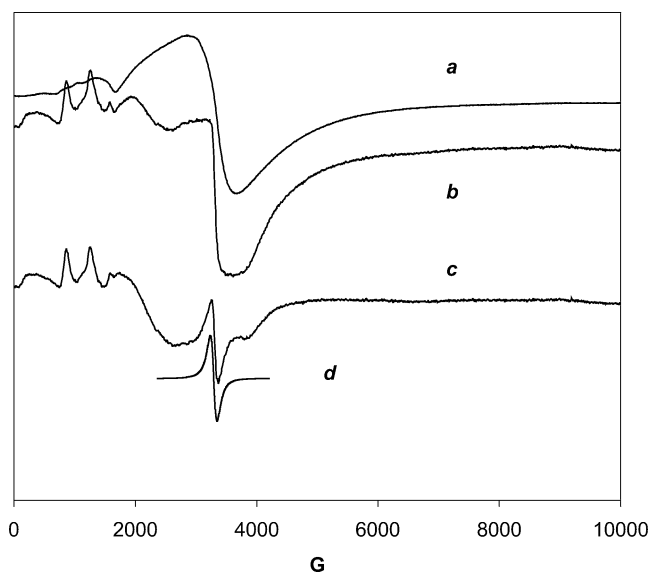


Fig. 3. (a) and (b) EPR spectra of Fig. 2a and 2b reported to the same intensity. (c) Difference between Fig. 3b and Fig. 3a. (d) Computer simulation of spectrum (c) with $g = 2.04$, peak to peak linewidth = 110 G, Lorentzian shape.

following the Curie law, indicating that such a line is due to paramagnetic entities sparsely dispersed within the sample. Hence, it has been attributed to traces of organic radicals, very likely coming from traces of the structure-directing agent still present in the catalyst. It cannot be excluded that this line was already present before the reduction, masked by the by far more intense patterns due to Fe³⁺ species. However, also the Fe³⁺–O–Fe²⁺ entities, formed by reduction of the binuclear Fe³⁺–O–Fe³⁺, extraframework, charge-compensating species, could contribute to the EPR spectrum of Fig. 2b and 2c. Indeed, the latter can be EPR silent as a result of the antiferromagnetic coupling between the two Fe³⁺ centers. However, if this binuclear species undergoes reduction to Fe³⁺–O–Fe²⁺, then the added electron can remain on one side of the couple and the residual Fe³⁺ can produce an EPR signal [21].

The structure of the active site for the benzene to phenol reaction is still an object of discussion. However, in a series of studies on the oxidation of methane and benzene on Fe-ZSM5, Panov et al. compared the structure of the active iron sites in ZSM5 to binuclear active centers in methane monooxygenase and suggested that they should be binuclear iron clusters. Furthermore, Mössbauer [3] and EXAFS [22] studies over Fe-ZSM5 zeolites pointed out the formation, during the postsynthesis thermal treatments, of binuclear Fe species, analogous to those found in the enzymatic monooxygenase. Therefore, this led us to consider that the peak observed at about 823 K is due to oxygen-bridged binuclear Fe clusters, charge-compensating the Fe³⁺ and Al³⁺ framework species and located at the ion-exchange positions of the zeolitic structure [22]. In our opinion these could be the species, called α -sites by Panov, possessing the ability of picking up oxygen from N₂O and releasing it

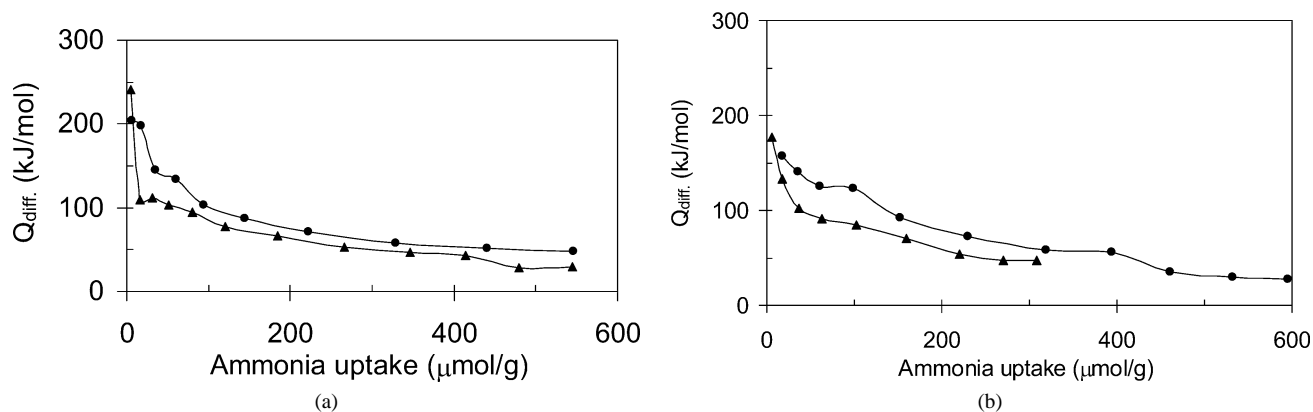


Fig. 4. (a) Differential heat of ammonia adsorption at 353 K for the Fe-Z(0.07) sample calcined at 823 (●) and 1073 K (▲), as a function of ammonia uptake. (b) Differential heat of ammonia adsorption at 353 K for the Fe-S(1.91) sample calcined at 823 (●) and 1073 K (▲), as a function of ammonia uptake.

to benzene, to form phenol, through a $\text{Fe}^{3+} \leftrightarrow \text{Fe}^{2+}$ redox mechanism.

Keep in mind that in the Fe-Z(x) catalysts the amount of charge-compensating extraframework iron is much higher than in the Fe-S(1.91) sample and increases with increasing iron content. This reflects the large difference in intensity of the peaks around 823 K, reflecting the difference in Al and Fe contents of these species. Indeed, with respect to Fe-S(x) samples, the Fe-Z(x) catalysts contain much less Fe, but much more Al, and the amount of charge-compensating Fe species roughly corresponds to the sum of the framework Al and Fe.

3.3. Surface acidity

Microcalorimetric data (see, e.g., Fig. 4a for Fe-Z(0.07)) revealed the presence of very strong acid sites after calcination at 1073 K. The initial value of the differential heat of adsorption Q_{diff} was 241 kJ/mol with Fe-Z(0.07) and 257 kJ/mol with Fe-Z(0.24). This value is comparable to those found with other zeolites [22].

The energy distribution, obtained by graphical derivation of the curves similar to those of Fig. 4a, reveals the existence of different sets of acid sites, each set being nearly homogeneous as to the strength. It is accepted [23,24] that calorimetric data can be employed to distinguish up to three families of acid sites, falling into proper energy intervals. In the present case, the region with Q_{diff} between 120 and 70 kJ/mol showed a high concentration of weak sites in Fe-Z(0.07) and a much lower concentration in Fe-Z(0.24). The interaction of NH_3 with acid sites was nonspecific below 70 kJ/mol, where ammonia tends to cluster with other ammonia molecules. Hence, the region with $Q_{\text{diff}} < 70$ kJ/mol was not considered any more. Therefore, strong acid sites (n_s , Table 2) were here considered as corresponding to $Q_{\text{diff}} > 120$ kJ/mol and weak acid sites (n_w) to $120 > Q_{\text{diff}} > 70$ kJ/mol.

The influence of calcination temperature on acidity of the Fe-Z(x) catalysts is typically shown in Fig. 4a for the Fe-Z(0.07) sample. At zero coverage, the differential heat

Table 2

Concentration of acid sites at 353 K. Strong (n_s): $Q_{\text{diff}} > 120$ kJ/mol and weak (n_w): $120 > Q_{\text{diff}} > 70$ kJ/mol, determined by microcalorimetry using NH_3 as probe molecule

Sample	n_s ($\mu\text{mol/g}$)	n_w ($\mu\text{mol/g}$)
Fe-Z(0.07)	21	176
Fe-Z(0.24)	48	150
Fe-Z(0.00) ^a	20	165
Fe-Z(0.01) ^a	22	160
Fe-S(0.30)	24	68
Fe-S(1.91)	35	157
Fe-S(0.00) ^a	21	59

^a Comparative samples.

of adsorption, for the sample calcined at 823 and 1073 K, was 204 and 241 kJ/mol, respectively, confirming that the treatment at higher temperature (1073 K) leads to the formation of stronger acid sites. It was demonstrated with various zeolites [25–28] that the interaction of the extraframework species (Lewis acid sites) with framework protonic sites (or silanol nests) significantly increases their acid strength. In agreement with the fact that the calcination at high temperature favors the migration of iron to extraframework positions [3–5], the existence of very strong sites is accompanied by the presence of a large amount of extraframework species as Fe-oxide and/or Al-oxide.

Total acidity decreased as the calcination temperature increased, confirming, as expected, that acidity is connected to the amount of accessible residual framework Fe (and Al), more than to the total amount of iron.

Calorimetric results for the Fe-S(x) samples calcined at 1073 K showed that the initial value of Q_{diff} was 177 kJ/mol with the Fe-S(1.91) catalyst, whereas it was 193 kJ/mol with the Fe-S(0.30). This indicates that acid sites are weaker with respect to Fe-Z(x) samples, in which framework aluminum is present in substantial amounts. Concentration of acid sites and acid strength distribution are reported in Table 2. Fig. 4b shows the effect of calcination temperature on the acidic properties of this catalyst. The initial value of Q_{diff} is 155 kJ/mol for the sample calcined at 823 K and 177 kJ/mol

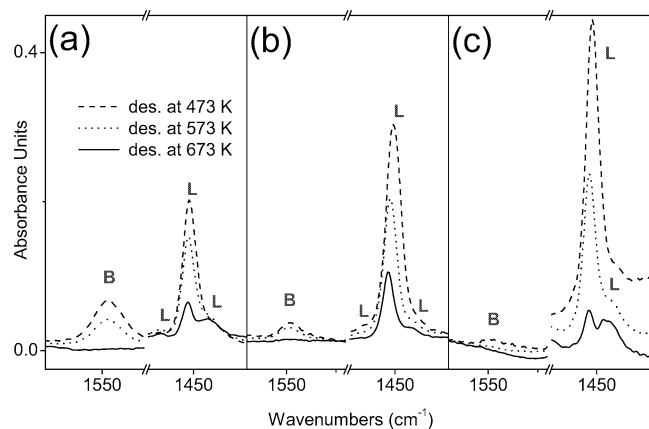


Fig. 5. IR spectra after pyridine saturation, followed by desorption at 473, 573, and 673 K, for the Fe-S(1.91) catalyst activated at 823 (a), 923 (b), and 1073 K (c).

for the sample calcined at 1073 K, in parallel with that observed with Fe-Z(*x*) samples (Fig. 4a).

The nature (and strength) of the acid sites was further investigated by FTIR, using pyridine as probe molecule. Pyridine sorption on acid sites resulted in the appearance of bands at 1548 cm^{-1} and at 1450 cm^{-1} , corresponding to pyridinium ions (PyrH⁺) and to pyridine coordinated to Lewis sites (PyrL), respectively. For brevity, this analysis is here reported in detail for the Fe-S(1.91) sample only. Fig. 5 shows the IR spectra recorded after pyridine desorption at 473, 573, and 673 K for the sample activated at 823 K (Fig. 5a), 923 K (Fig. 5b), and 1073 K (Fig. 5c). Comparison of the three experiments shows that the concentration of Brønsted acid sites (band at 1548 cm^{-1}) decreased with increasing activation temperature. A weak adsorption at 1548 cm^{-1} was observed also after activation at 1073 K, indicating that some iron is still in framework position. Pyridine sorption on Lewis sites resulted in the appearance of three different bands at 1462, 1452, and 1444 cm^{-1} . After pyridine desorption at 473 K, the band at 1452 cm^{-1} had the highest intensity, with a frequency near to that generally observed after pyridine desorption from zeolites containing extraframework aluminum species (Al³⁺) [25,29,30]. Hence, this band can be assigned to extraframework iron species (Fe³⁺), whose concentration increases with increasing treatment temperature. The weak band at 1462 cm^{-1} was often observed also in Al-containing zeolites and assigned to a second kind of Lewis acid sites with a greater acid strength [25,29,30]. The band at 1444 cm^{-1} is new for these systems. This band was observed at the same wavenumber as the band corresponding to pyridine hydrogen-bonded to silanols [31], but its presence also after desorption at 673 K allows us to exclude that it is about a simple hydrogen bond. It should be emphasized that this band corresponds to a third Lewis extraframework site with a milder acidity. According to our previous data [8], obtained by means of XANES and IR spectroscopy, the band at 1444 cm^{-1} can be attributed to extraframework Fe²⁺ species.

Table 3

Concentration of Brønsted (PyrH⁺) and of Lewis (PyrL) acid sites in Fe-S(1.91) catalyst, activated at 823, 923, and 1073 K, determined by FTIR spectroscopy after pyridine adsorption

Sample	T (K)	PyrH ⁺ (μmol/g)	PyrL (μmol/g)
Fe-S(1.91) ₈₂₃	473	98.8	200
	573	55.4	148
	673	–	60.3
Fe-S(1.91) ₉₂₃	473	32.8	316
	573	23.0	186
	673	–	87.4
Fe-S(1.91) ₁₀₇₃	473	8.4	373
	573	1.7	227
	673	–	85.9

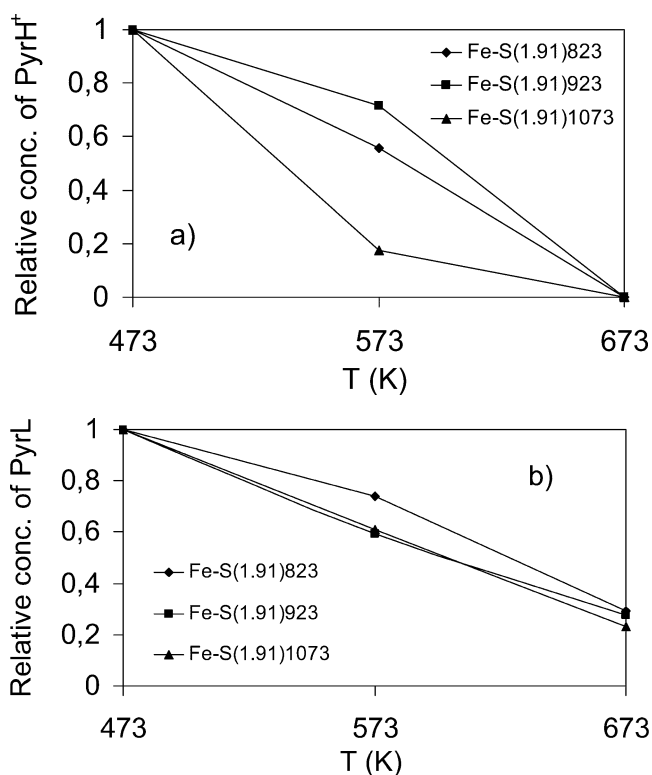


Fig. 6. Change in the relative concentration of pyridinium ions (PyrH⁺) (a) and of pyridine bound to Lewis acid sites (PyrL) (b) vs desorption temperature.

The concentration of Brønsted and Lewis acid sites was estimated, as noted, by using the values of molar extinction coefficients reported in [11]. The results are summarized in Table 3. Whatever the treatment of the sample, the number of Lewis sites able to retain pyridine at 473 K was higher than the number of protonic sites: by 1.5 times for Fe-S(1.91)₈₂₃, 6.5 times for Fe-S(1.91)₉₂₃, and 27 times for Fe-S(1.91)₁₀₇₃. However, pyridine desorbed less easily from Lewis sites (Fig. 6b) than from Brønsted sites (Fig. 6a), which can therefore be considered as weaker. The concentration of Lewis sites increased with increasing treatment temperature, hence with the increase of extraframework iron. In fact, after activation at 823 K, a considerable percentage of Lewis

sites (equal to 53% of the amount titrated after activation at 1073 K) was already present.

3.4. Catalytic activity

Catalytic activity has been expressed as mol% conversion of benzene and mol% selectivity to phenol. Phenol, together with some water, was usually the main product in the reactor effluent collected in the refrigerated sampling trap. Only at high temperature (> 673 K) small amounts of by-products (mainly benzoquinone and benzofuran) were detected. Total oxidation of benzene to carbon dioxide and water was the main undesired reaction.

3.4.1. Fe-Z(x) catalysts

Fig. 7a shows the results obtained with the Fe-Z(0.07) sample under atmospheric pressure. The increase of temper-

ature from 623 to 673 K increased the initial (1 h on-stream) conversion by 2.5 times, while an increase by 6 times was observed when raising the temperature from 623 to 723 K.

More or less rapidly all the zeolites underwent deactivation, more pronounced at short values of time-on-stream. Activity decay was due to coking, as reported also by others [32]. Removing coke by burning out in air flow resulted in the full recovery of catalytic activity. The decrease in conversion and the almost complete deactivation of the catalyst within 6 h on-stream can therefore be ascribed to the production of phenol and polyphenols, which are well-known coke precursors. The higher the temperature, the faster the deactivation, due to the effect of temperature both on the rate of coke precursor formation and on their transformation into heavier and heavier species. It is known [33,34] that at low temperatures the rate of coking is due to the easier retention of coke in the zeolite pores, because of their low volatility

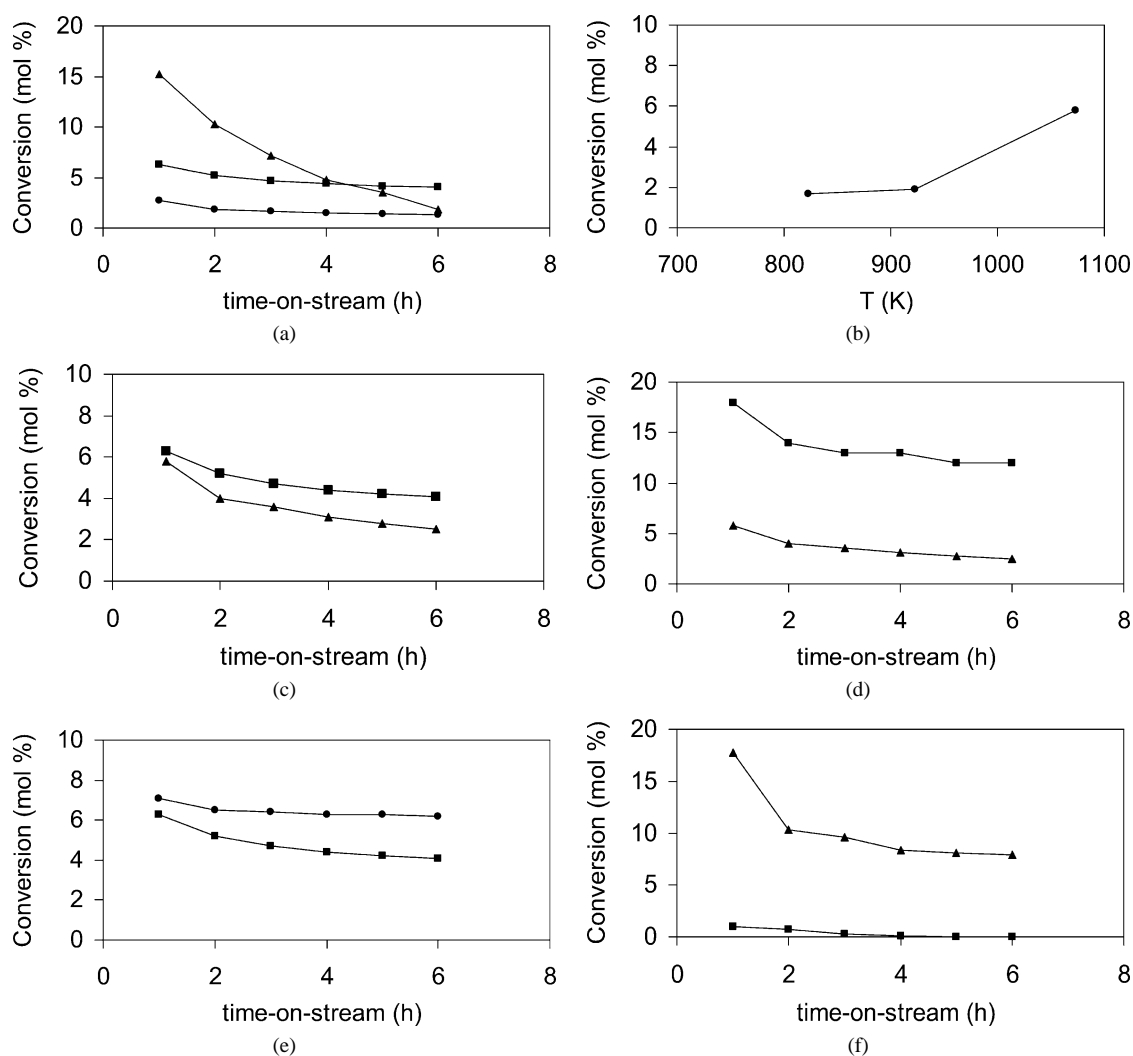


Fig. 7. (a) Influence of reaction temperature on conversion for the Fe-Z(0.07) sample. $T = 623$ (●), 673 (■), and 723 K (▲). Feed: benzene: $1 \text{ cm}^3/\text{h}$ (liq), N_2O : $17.9 \text{ cm}^3/\text{min}$, He: $62.5 \text{ cm}^3/\text{min}$; $\tau = 0.5$ s. (b) Initial conversion at 673 K vs calcination temperature for the Fe-Z(0.07) sample. (c) Conversion vs time-on-stream for the Fe-Z(0.07) (■) and Fe-Z(0.24) (▲) catalysts; $T = 673$ K. (d) Conversion at 673 K vs time-on-stream for the Fe-Z(0.24)catalyst: (▲) calcined at 1073 K, (■) steamed at 873 K for 5 h. (e) Influence of steam on conversion at 673 K. Fe-Z(0.07) catalyst: (■) without steam addition and (●) with steam addition. (f) Conversion at 673 K vs time-on-stream for the Fe-S(0.30) (■) and Fe-S(1.91) (▲) catalysts.

and their adsorption proneness, while at high temperatures coking is due mainly to the high rate of formation of precursors, so that catalyst decay is due to highly polyaromatic molecules trapped within the zeolite pores.

In the present study we chose to work at 673 K, due to a better performance of catalyst in terms of lower deactivation rate and better stability. Benzene conversion increased with increasing calcination temperature (Fig. 7b), while the selectivity was shown to be rather independent of this parameter, always being higher than 90%. Activity growth with calcination temperature can be explained with the migration of iron into the extraframework position, creating the active species for the present reaction [1,3–5, 8,35,36].

Fig. 7c compares the conversion of benzene as a function of time-on-stream for the Fe-Z(*x*) catalysts calcined at 1073 K. The more rapid deactivation of Fe-Z(0.24) can be ascribed to fast formation of coke, probably due [37] to its very strong acid sites (initial $Q_{\text{diff}} = 257$ kJ/mol, vide supra), whereas the increase in the iron percentage on the catalyst from 0.07 to 0.24 wt% seems to influence appreciably neither the initial catalytic activity (ca. 6%) nor the selectivity to phenol.

A very strong increase in catalytic activity was observed after steaming of the catalysts. A comparison for the Fe-Z(0.24) sample, calcined at 1073 K or treated at 873 K for 5 h in a stream of air +30–50% steam, is shown in Fig. 7d. Steaming increases initial conversion by 3 times with respect to simple calcination at high temperatures. Furthermore, deactivation was lower and after 2 h on-stream conversion tended to level off to about 80% of the initial value. Steaming then appears to be a more effective method, with respect to treating at high temperatures in dry gas, in favoring the migration of iron to extraframework positions, so creating a larger amount of active species for the hydroxylation of benzene.

To investigate the possibility of improving catalyst performance, some comparison runs were carried out at 673 K on Fe-Z(*x*) zeolites, calcined at 1073 K, by adding some water (partial pressure = 17 Torr) to the fresh feed, with appropriate changes in the inert (helium) partial pressure, to keep unchanged the partial pressure of benzene (37 Torr) and of N₂O (162 Torr). Water addition improved both activity and selectivity with respect to the dry feeding and increased also the stability of the catalyst (Fig. 7e). Indeed, the residual activity, defined as the ratio between conversion values at 6 h and at 1 h on-stream, was about 65% when the reaction was carried out with dry feed, while it attained about 90% when adding steam. The positive role played by steam on the catalytic behavior of Fe-Z(*x*) catalysts can be ascribed to the continuous cleaning up of the catalyst surface. Indeed, the total amount of coke deposited on the Fe-Z(*x*) zeolites when working with dry feeding was considerably higher than that deposited when adding water. For example, for the Fe-Z(0.07) sample, total coke amounted to 11.1 wt% and to 9.5 wt%, respectively, after 6 h on-stream.

Total acidity seems not to influence dramatically the initial activity. In fact, despite a relatively large difference in concentration of strong acid sites of the Fe-Z(*x*) samples (Table 2), similar values of initial conversion (ca. 6%) were measured for the two catalysts (Fig. 7c).

These data have been confirmed by some catalytic tests carried out on the two comparative samples of H-ZSM5 zeolite, the first one (Fe-Z(0.00), Table 1) synthesized in the virtual absence of iron (less than 0.005 wt% Fe₂O₃, corresponding to the lower detection limit of our ICP apparatus) and the second (Fe-Z(0.01), Table 1) synthesized in the presence of traces of iron, but both characterized by an acidity similar to that of the Fe-Z(0.07) sample (Table 2). The first catalyst was totally inactive, while the second gave an initial conversion of 2% only and a selectivity to phenol > 90%, showing once again that the catalytic activity is practically unaffected by acidity and it is tightly connected with the presence of iron. Indeed, the formation of phenol takes place in the presence of the Fe-based centers only. Once formed, phenol may undergo a more or less rapid decomposition-condensation (vide infra), leading to catalyst coking, the rate of which depends on the strength of surface acid sites. The latter then govern the coke formation rate only, showing completely inactive in the absence of phenol, at least under the reaction conditions usually selected for the present main process.

3.4.2. Fe-S(*x*) catalysts

As found for the Fe-Z(*x*) catalysts, the conversion of the Fe-S(*x*) samples increased with increasing calcination temperature, due to the increasing extraction of framework Fe. For brevity, we here report the catalytic behavior of the Fe-S(*x*) samples (Fig. 7f) for the best pretreating temperature (1073 K) and at the standard reaction temperature (673 K), as a function of time-on-stream. For both catalysts, conversion decreased during the first 3 h on-stream and then stabilized, while the selectivity was always higher than 90%. The increase of iron percentage from 0.30 to 1.91 wt% led to an increase of initial activity of 18 times. In addition, it was confirmed that the presence of aluminum in the framework lowers by ca. one order of magnitude the percentage of iron needed for obtaining an active catalyst [35].

Once again a virtually ironless sample (Fe-S(0.00), Table 1, with less than 0.005 wt% Fe₂O₃) was inactive, whereas the Fe-S(0.30) sample, containing 0.30% Fe₂O₃ only, already showed a weak activity, attaining an initial conversion of ca. 2%. However, when feeding water together with benzene over the Fe-S(1.91) sample, no significant change in catalytic activity was observed, at difference with what was noted in the case of Fe-Z(*x*) samples. This is likely due to the different hydrophilicity of the two catalysts.

Finally, the increase of Lewis acid sites concentrations with increasing pretreatment temperature (vide supra) paralleled the increase of extraframework iron species and hence of catalytic activity. By contrast, the concentration of Brønsted acid sites decreased with increasing pretreatment

Table 4
Amount of soluble and insoluble coke for the Fe-Z(*x*) samples after 6 h on stream

Sample	C_{sol} (wt%)	C_{insol} (wt%)
Fe-Z(0.07)	2.53	8.57
Fe-Z(0.24)	0.88	14.38

temperature (Table 3), showing clearly that they are not responsible for catalytic activity for the main reaction.

3.5. Catalyst deactivation

Coke formation was investigated during benzene hydroxylation at 673 K over the Fe-Z(*x*) samples after 6 h on-stream. Results are collected in Table 4. More than 90% of coke consisted of insoluble matter, i.e., high molecular weight (MW) unextractable substances, whereas the soluble coke, as shown by GC-MS analysis, consisted of phenol and simple or condensed polyphenols and products derived from further condensation. The coke components could be classified into seven (A to G, Table 5) families, with $C_nH_{2n-z}O_x$ as general formula.

When the pore system consists of interconnecting channels without cavities, as in the ZSM5 framework, deactivation occurs first through limitation of the access to the active sites and then by blockage of the access to the sites of the channel intersection in which the coke molecules are sitting. In fact, it is known [37] that in MFI zeolites the soluble coke molecules remain trapped into the micropores (pore size < 20 Å), so that deactivation is due essentially to the formation of *emboli*, preventing any further access of reactants to the inner part of the pores. However, in the present case the distribution of pore volume, as micro and mesopores (Table 1), shows that very likely the coke forms and grows not only in micropores, but also in mesopores. In fact, in our catalysts coke is prevalently made of high MW polyaromatics, which can find room for growing first at channel intersections only. Then they continue to grow at the pore mouth, i.e., on the external surface of the zeolite crystals, but within the intercrystalline, intraparticle mesopores.

The total amount of coke (ca. 15 wt%) and especially of insoluble coke (more than 14 wt%), deposited on the Fe-Z(0.24) sample, was higher than that deposited on the Fe-Z(0.07) sample (Table 4). Indeed, the more than double concentration of strong acid sites of the Fe-Z(0.24) sample, with respect to Fe-Z(0.07) (Table 2), leads not only to a quicker deactivation, but also to a quicker hardening of the carbonaceous deposits.

The amount of coke deposited over the Fe-S(1.91) sample was determined also for different time-on-stream values (Table 6). The solubility of coke in methylene chloride (C_{sol}) decreased with increasing time-on-stream, i.e., with the increase of coke amount. Initially, virtually all the coke was soluble, whereas after 1 h on-stream the main part of coke consisted of higher MW polyaromatic compounds and so it became insoluble (Fig. 8 and Table 6). Finally, GC-MS

Table 5
Main components of soluble coke

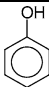
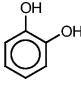
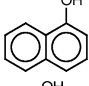

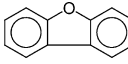
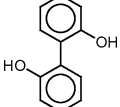
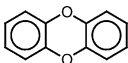
Family	General formula	Typical coke molecule	Developed formula
A	$C_nH_{2n-6}O$	Phenol	
B	$C_nH_{2n-6}O_2$	1,2-Benzenediol	
C	$C_nH_{2n-12}O$	1-Naphthol	
D	$C_nH_{2n-14}O$	[1,1'-Biphenyl]-2-ol [1,1'-Biphenyl]-3-ol [1,1'-Biphenyl]-4-ol	
E	$C_nH_{2n-16}O$	Dibenzofuran	
F	$C_nH_{2n-14}O_2$	[1,1'-Biphenyl]-2,2'-diol	
G	$C_nH_{2n-16}O_2$	Oxanthrene	

Table 6
Coke composition in the Fe-S(1.91) sample at different time-on-stream values

Time-on-stream (h)	1	6	72
C_{tot} (wt%)	7.5	12.6	15.1
C_{sol} (wt%)	1.2	0.5	–
C_{insol} (wt%)	6.3	12.1	15.1

analysis of the coke deposited over Fe-S(*x*) samples revealed the same nature of components and the same distribution of the soluble (10 wt%) and insoluble (90 wt%) coke found for the Fe-Z(*x*) samples.

For the Fe-S(*x*) samples too the dependence of deactivation rate on concentration of strong acid sites mimicked that observed for the Fe-Z(*x*) catalysts (vide supra). Indeed, the Fe-S(1.91) catalyst, possessing a much higher concentration of strong acid sites, with respect to Fe-S(0.30) (Table 2), deactivated much more rapidly (Fig. 7f).

4. Conclusions

The most important conclusions one can draw from the present results can be briefly summarized as follows:

- In the total absence of Fe virtually no activity was observed, both for the desired reaction and for any other reaction accompanying the main one. This means that phenol formation can take place on Fe-based sites only.

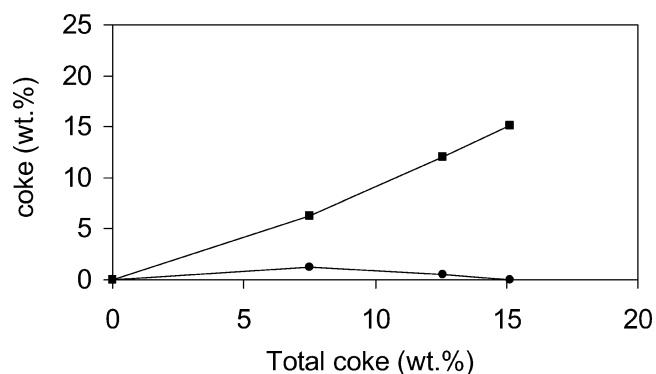


Fig. 8. Change in the amount of soluble (●) and insoluble (■) coke vs total coke formed. Fe-S(1.91) catalyst, reaction conditions as in Fig. 7.

- (ii) These active sites could very likely be composed of oxygen-bridged, extraframework, binuclear Fe species, charge-compensating the framework Fe^{3+} or Al^{3+} ions, able to pick up oxygen from N_2O and to release it to benzene, to form phenol, through a $\text{Fe}^{3+} \rightleftharpoons \text{Fe}^{2+}$ redox mechanism.
- (iii) Catalyst deactivation derived mainly from the decomposition-condensation of phenol onto acid sites, the stronger being the latter, the quicker being the coking rate. In other words, surface acidity was not responsible for activity in the main reaction, but it was heavily involved in catalyst deactivation by coking.
- (iv) For Fe-Z(x) samples, addition of steam to the feed improved substantially activity, selectivity, and mainly durability of the catalyst, very likely due to an efficient cleaning up of the catalyst surface from carbonaceous deposits.

Acknowledgments

The financial support of Italian Ministry of University and Scientific and Technological Research (MURST), through the COFIN 2000 program, is gratefully acknowledged. We are indebted to O. Ballabio for collecting the EPR data.

References

- [1] A.K. Uriarte, M.A. Rodkin, M.J. Gross, A.S. Kharitonov, G.I. Panov, *Stud. Surf. Sci. Catal.* 110 (1997) 857.
- [2] E. Suzuki, K. Nakashiro, Y. Ono, *Chem. Lett.* 6 (1988) 953.
- [3] G.I. Panov, A.K. Uriarte, M.A. Rodkin, V.I. Sobolev, *Catal. Today* 41 (1998) 365.
- [4] V.I. Sobolev, G.I. Panov, A.S. Kharitonov, V.N. Romannikov, A.M. Volodin, K.G. Ione, *J. Catal.* 139 (1993) 435.
- [5] L.V. Pirutko, V.S. Chernyavsky, A.K. Uriarte, G.I. Panov, *Appl. Catal. A: Gen.* 227 (2002) 143.
- [6] R. Burch, C. Howitt, *Appl. Catal. A: Gen.* 103 (1992) 135.
- [7] R. Leanza, I. Rossetti, I. Mazzola, L. Forni, *Appl. Catal. A: Gen.* 205 (2001) 93.
- [8] G. Berlier, G. Spoto, S. Bordiga, G. Ricchiardi, P. Fiscicaro, A. Zecchina, I. Rossetti, E. Selli, L. Forni, E. Giamello, C. Lamberti, *J. Catal.* 208 (2002) 64.
- [9] A.M. Ferretti, C. Oliva, L. Forni, G. Berlier, A. Zecchina, C. Lamberti, *J. Catal.* 208 (2002) 83.
- [10] V. Solinas, I. Ferino, *Catal. Today* 41 (1998) 179.
- [11] E. Selli, L. Forni, *Micropor. Mesopor. Mater.* 31 (1999) 129.
- [12] P. Magnoux, P. Roger, C. Canaff, V. Fouché, N.S. Gnep, M. Guisnet, *Stud. Surf. Sci. Catal.* 34 (1987) 317.
- [13] J.L. Motz, H. Heinichen, W.F. Hölderich, *J. Mol. Catal. A: Chem.* 136 (1993) 175.
- [14] H. Van Koningsveld, *Stud. Surf. Sci. Catal.* 58 (1991) 35.
- [15] P. Ratnasamy, R. Kumar, *Catal. Today* 9 (1991) 329.
- [16] S. Bordiga, R. Buzzoni, F. Geobaldo, C. Lamberti, E. Giamello, A. Zecchina, G. Leofanti, G. Petrini, G. Tozzola, G. Vlaic, *J. Catal.* 158 (1996) 486.
- [17] Q. Kan, Z. Wu, R. Xu, Q. Wei, S. Peng, G. Xiong, S. Sheng, J. Huang, in: P.A. Jacobs, N.I. Jaeger, L. Kubelková (Eds.), *Zeolite Chemistry and Catalysis*, Elsevier, Amsterdam, 1991, p. 241.
- [18] E. Dumitriu, V. Hulea, I. Fechet, A. Auroux, J. Lacaze, C. Guimon, *Micropor. Mesopor. Mater.* 43 (2001) 341.
- [19] El-M. El-Malki, R.A. van Santen, W.M.H. Sachtler, *J. Catal.* 186 (2000) 212.
- [20] A.V. Kucherov, A.A. Slinkin, *Zeolites* 8 (1988) 110.
- [21] M.C.R. Symons, F.A. Taiwo, D.A. Svistunenko, *J.C.S. Faraday Trans.* 89 (1993) 3071.
- [22] P. Marturano, L. Drozdová, A. Kogelbauer, R. Prins, *J. Catal.* 192 (2000) 236.
- [23] N. Cardona-Martinez, J.A. Dumesic, *Adv. Catal.* 38 (1992) 149.
- [24] N. Cardona-Martinez, J.A. Dumesic, *J. Catal.* 136 (1992) 392.
- [25] A.K. Ghosh, G. Curthoys, *J. Chem. Soc. Faraday Trans. I* 79 (1983) 805.
- [26] S. Morin, A. Berreghis, P. Ayrault, N.S. Gnep, M. Guisnet, *J. Chem. Soc. Faraday Trans.* 93 (1997) 3269.
- [27] C. Mirodatos, D. Barthomeuf, *J. Chem. Soc., Chem. Comm.* (1981) 39.
- [28] F. Lonyi, J.H. Lunsford, *J. Catal.* 136 (1992) 566.
- [29] P.A. Jacobs, J.B. Uytterhoeven, *J. Catal.* 26 (1972) 175.
- [30] A. Vimont, F. Thibault-Starzyk, J.C. Lavalley, *J. Phys. Chem. B* 104 (2000) 286.
- [31] R. Buzzoni, S. Bordiga, G. Ricchiardi, C. Lamberti, A. Zecchina, G. Bellussi, *Langmuir* 12 (1996) 930.
- [32] M. Häfele, A. Reitzmann, D. Roppelt, G. Emig, *Appl. Catal. A: Gen.* 150 (1997) 153.
- [33] M. Guisnet, P. Magnoux, in: E.G. Derourane, F. Lemos, C. Naccache, F.R. Ribeiro (Eds.), *Zeolite Microporous Solids: Synthesis, Structure and Reactivity*, in: NATO ASI Series C, Vol. 352, Kluwer, Dordrecht, 1992, p. 437.
- [34] H.G. Karge, *Stud. Surf. Sci. Catal.* 58 (1991) 531.
- [35] A.S. Kharitonov, G.A. Sheveleva, G.I. Panov, V.I. Sobolev, Y. Paukshtis, V.K. Romannikov, *Appl. Catal. A: Gen.* 98 (1993) 33.
- [36] K.A. Dubkov, V.I. Sobolev, G.I. Panov, *Kinet. Catal.* 39 (1998) 72.
- [37] M. Guisnet, P. Magnoux, D. Martin, *Stud. Surf. Sci. Catal.* 111 (1997) 1.